Title: Oncostreams: Self-organization and dynamics determine spatial heterogeneity and malignant behavior in gliomas

Andrea Comba[1,2,4], Sebastien Motsch[3], Patrick J. Dunn[1,2,4], Todd C. Hollon[1], Daniel B. Zamler[1,2,4], Anna E. Argento[1,2], Celina G. Kleer[4,5], Maria G Castro[1,2,4], and Pedro R. Lowenstein[1,2,4,*]

[1]Dept. of Neurosurgery, University of Michigan Medical School, Ann Arbor, 48109, MI, USA
[2]Dept. of Cell and Developmental Biology, University of Michigan Medical School, Ann Arbor, 48109 MI, USA
[3]School of Mathematical and Statistical Sciences, Arizona State University, Tempe, AZ, USA
[4]Rogel Cancer Center, University of Michigan medical School, Ann Arbor, 48109, MI, USA
[5]Dept. of Pathology, University of Michigan Medical School, Ann Arbor, MI 48109, USA
*Correspondence to: pedrol@umich.edu

Abstract

Tumor heterogeneity is a hallmark of cancer and a determinant of malignant behavior. How tumor heterogeneity arises is thus of fundamental importance. Gliomas display oncostreams, self-organizing multicellular fascicles of elongated, aligned, collectively motile glioma cells, that establish dynamic heterogeneity throughout gliomas. Gliomas exhibit two collective motion patterns: streams, displaying bidirectional collective motion, and flocks, displaying unidirectional collective motion. Oncostreams function as highways to facilitate the intratumoral spread of tumoral and non-tumoral cells. Detailed quantitative and deep learning analysis of rodent and human gliomas uncovered that the density of oncostreams correlates positively with glioma aggressiveness. Our study establishes the self-organizing dynamic nature of gliomas, and its role in setting up dynamic tumor heterogeneity and consequently tumor malignant behavior.

INTRODUCTION

Tumor heterogeneity is a characteristic hallmark of cancer that is thought to determine tumor malignant behavior and treatment resistance. Glioma spatial heterogeneity can be detected at the histological, molecular, and cellular level (*1-4*). We uncovered the existence of dynamic heterogeneity. The organization of gliomas is highly dynamic, and is structured into diverse self-organizing patterns of collective motion named "oncostreams". These patterns of self-organization correlate with tumor malignancy in rodent and human gliomas, suggesting a causal pathological role for glioma self-organization and dynamic heterogeneity.

We demonstrate the existence of oncostreams or dynamic fascicles of elongated glioma cells, that self-organize into patterns of collective motion such as streams and flocks. We demonstrate the neuropathological characteristics of oncostreams, their highly dynamic nature, their correlation with tumor malignant behavior, their functional role in tumor invasion and progression, and their potential causal role in setting up tumor spatial heterogeneity. We propose that glioma self-organization facilitates the emergence of dynamic tumor behaviors that determine malignant growth, and could thus become targets for novel treatments.

RESULTS

Intra-tumoral self-organized collective motion dynamics in glioma tumors

Gliomas are characterized by prominent cellular, molecular, and spatial heterogeneity; a role of dynamics in tumor heterogeneity, however, remains unknown. We uncovered surprising widespread dynamics of glioma cells throughout the glioma mass, as predicted by our agent-based model (**Fig. 1A**) (*5*). To investigate these dynamics, we established a physiologically viable organotypic brain slice model. The movement of glioma cells expressing green fluorescent protein (GFP) was visualized using time-lapse confocal imagining, and tracked using Fiji's plug-in Track-Mate **(Fig. 1, B to D).**

The glioma tumor core displays groups of cells (zones) with similar nematic orientation (**Fig. 1E and Fig. S1F**) and which resemble collective motion (*6-11*). To characterize patterns of collective motion we determined the cells' angle velocity, velocity vector and speed within each zone (**Fig. 1, E to J and Fig. S1G**). Angle velocity distribution indicated the existence of three patterns of collective motility (**Fig. 1G**): in 'Zone a' cells don't have a preferred direction, in 'Zone b' cells move in opposite directions (~ 135° and 315°), and in 'Zone c' all cells move with a single similar preferred direction (~ 45°) (**Fig. 1, G and H).** These analyses disclosed three types of patterns of collective motion, which we denote by 's*warm*' (Zone a), '*stream*' (Zone b), or '*flock*' (Zone c).

Further, we established a robust criterion to classify these migratory patterns: we used the distribution of all angle velocity values θ_i to determine the likelihood of any experimental distribution being either a *stream*, a *flock*, or a *swarm*. The distribution of the angle velocity is constant in a *swarm* (all angle velocities are equally probable), bi-modal in a *stream* (cells are moving in both directions), and uni-modal in a *flock* (**Fig. 1, I and J)**. The likelihood analysis demonstrates that 'Zone a' illustrates a *swarm*, 'Zone b' a *stream*, and 'Zone c' a *flock* (**Fig. 1J**).

The Akaiki Weight (AW) indicates which pattern has the highest likelihood in each experimental situation. Speed differed among the three dynamic patterns (**Fig. 1F, and Fig. S2B, S3B S4B, and S17 A**). Taking a threshold of 2μm/h, the cells inside a flock or stream move faster than the threshold 83% of the time, and inside a swarm they move 71.2% of the time.

The statistical analyses suggest that glioma cells move by collective motion in a manner resembling the movements of self-organizing flocks of birds (*12*). Because local pairwise interactions among individuals are sufficient to propagate the order throughout the flock we determined the internal organization of the cells by pair-wise correlation analysis (relative position and pair correlation) by tumor zones (**Fig. 1K and Fig. S1 C to E**). We observed that within *swarms*' cells are more separated, and the relative position of the nearby neighbors is 20-40 μm. *streams* and *flocks* have higher density, and the nearby neighbors are closer (at 20-30 μm) (**Fig. 1L and Fig. S2F, S3F and S4F**). Pair-wise correlation with nearby neighbors showed that cell movement is positively correlated in all patterns at distances between 10-50 μm, with higher correlation left-right for *streams* (≈0.2), left-right/front-back for *flocks* (≈0.2-0.4), and a lower correlation for *swarms* (≈0.1) (**Fig. 1M and Fig. S2G, S3G and S4G).** This study of glioma tumors are compatible with the results of Ralitza *et al*. (*13*), indicating the possible existence of tumor dynamics across a larger variety of tumor types.

Thus, our analyses strongly suggest that glioma tumors are dynamically heterogeneous and display self-organizing collective migratory behavior such as *streams* and *flocks*.

Oncostreams: multicellular fascicles of elongated tumor cells in mouse and human gliomas

To determine whether glioma collective motion patterns have a morphological correlate we performed histological analyses of H&E sections taken from imaged organotypic slices. **Fig. 2A and B** illustrates a histological section taken from the organotypic slice shown in **Fig. 1, C to E**. In correlated histological sections we could identify well-defined histological areas formed by elongated and aligned cells whose eccentricity and alignment matched the dynamic imaging results. Cells within histological areas corresponding to *streams* and *flocks* have an aspect ratio of 2.2 and 2.7 respectively (i.e., elongated cells), while those within areas corresponding to *swarms* have cells with an aspect ratio of 1.2 (i.e., round cells) **(Fig. 2, B and C)**. As predicted by our *in silico* model (*5*) these results suggest that cell shape, or eccentricity, is involved in the organization of collective motion patterns.

Elongated cells within *streams* and *flocks* are nematically aligned with each other, i.e., they move in the same or opposite direction, whereas round cells within *swarms* are not **(Fig. 2D).** Therefore, taking into account the cellular shape and angle orientation, we define such multicellular structures, as '*oncostreams'* (i.e., *streams* or *flocks*). Notice that only the dynamic analysis of collective motion can differentiate between *streams* and *flocks*. *Oncostreams* are thus defined as fascicles of aligned and elongated cells (≈5-30 cells wide) which at the dynamic level are defined as *streams* or *flocks*.

To study whether oncostreams exist in other mouse glioma models as well in human glioma specimens we examined histological sections from various tumor types **(Fig. 2, E and F).** We determined the existence of *oncostreams* in mouse genetic models of glioma as NPA (Nras, shP53, shATRx) and NPD (Nras, shP53, PDGFβ) and in the GL26 glioma cells implantable models (**Fig. 2E**). Moreover, human glioma biopsies and a xenograft glioma model (SJGBM2) demonstrated the presence of these organized multicellular *oncostreams* in human tissue (**Fig. 2F**). Analysis of cell eccentricity and alignment validated these structures as *oncostreams* **(Fig. 2, G and H and Fig. S5).** Our data thus indicate that a comprehensive study of tumors including histological, morphological and dynamic data enable a thorough classification of collective motion in gliomas.

The presence of oncostreams correlates with tumor malignancy in mouse glioma models and glioma patients

To understand whether *oncostream* density correlates with tumor aggressiveness and clinical outcomes we generated genetically engineered tumors of different malignant behavior using the Sleeping Beauty Transposon system **(Fig. 3A)** (*4, 14, 15*). We induced tumors harboring two different genotype combinations: (I) NRAS pathway activation in combination with shp53 and shATRX downregulation (**NPA**), and, (II) NRAS activation, shp53 downregulation, shATRX downregulation, and mutant IDH1-R132 expression (**NPAI**) **(Fig. 3A)**. IDH1-wild-type tumors (**NPA**) display a highly malignant phenotype and worst prognosis (MS: 70 days), compared with tumors harboring the IDH1R132R mutation, **NPAI,** (MS: 213 days) **(Fig. 3B)**. This outcome reproduces human gliomas, where patients with IDH1-mutant tumors have prolonged median survival (*16, 17*). Histopathological analysis of these tumors showed a positive correlation between the presence of *oncostreams* and tumor malignancy **(Fig. 3C)**. NPA tumors exhibited large areas of *oncostreams* **(Fig. 3C and Fig. S8)** within a highly infiltrative and heterogeneous glioma

characterized by abundant necrosis, microvascular proliferation, and cellular heterogeneity as described before (*14, 15, 18*).

To objectively determine *oncostream* density we trained a fully convolutional neural network (fCNN) to identify and quantify tumor areas covered by *oncostreams* (**Fig. 3C and Fig. S6 and S7 A**). Our deep learning analysis found that within NPA tumors oncostreams occupied 15.28 ± 6.105% of tumor area compared with 1.18 ± 0.81 % in NPAI tumors (**Fig. 3 C and D, and Fig. S8 A and B**). Cellular alignment correlated with the presence or absence of *oncostreams* (**Fig. 3E**).

To determine whether *oncostream* organization correlates with glioma aggressiveness in human patients we evaluated a large cohort of TCGA glioma diagnostic slides from the Genomic Data Commons Portal of the National Cancer Institute. We manually analyzed 100 TCGA-glioblastoma multiforme tissue sections (WHO Grade IV) and 120 TCGA-low grade glioma tissues (WHO Grade II and III) using the slide image viewer of the portal (**Table 1**). *Oncostreams* were present in 47% of TCGA-GBM grade IV tumor tissues, in 8.6 % of TCGA-LGG grade III, and were absent in TCGA-LGG grade II (**Fig. 4A and Table S2**). To validate our identification of *oncostreams* we examined the H&E images using our deep learning algorithm. We observed a strong concordance (>84%) between machine learning and our visual identification of *oncostreams* (**Table S4)**. Oncostreams presence/absence and its segmentation by deep learning is illustrated in **Fig. 4B and Fig. S9A and S10 A and B**. Additionally, eccentricity and alignment analysis of glioma cells confirm the existence of oncostreams in human tissue (**Fig. 4C**). The median survival analysis of the selected cohort are consistent with the Gliovis brain tumor data-sets portal (http://gliovis.bioinfo.cnio.es) (**Fig. S10C**). Thus, our deep learning algorithm validates our visual histological identification of *oncostreams* in H&E glioma images.

Patterns of self-organized collective motion: cell-heterogeneity and intratumoral distribution of non-tumor cells by *oncostreams*

To gain insight into the biological functions of oncostreams we asked if oncostreams are homogeneous or heterogeneous structures. In mouse and human glioma tumors, oncostreams are formed by GFP+ and Sox2+ tumor cells, and also contain non-tumoral cells such as cells expressing Nestin+ stem cells, GFAP+ cells, Iba1+ microglia/macrophages cells, and ACTA2+

mesenchymal cells (**Fig. 5, A and B, and Fig. S11 A to C**). Alignment analysis showed a positive alignment of non-tumoral cells with *oncostream* cells (**Figure 5A-B**).

Human high-grade gliomas displayed GFAP+ astrocytes and Iba1+ macrophage/microglial cells aligned with SOX2+ tumor cells along *oncostreams*. Low grade gliomas did not contain *oncostreams* (**Fig. 5, B and C**). The negative staining for neurofilaments (Neurofilament-L) strongly suggests that oncostreams are not organized along brain axonal pathways **(Fig. S12A)**. *Oncostreams* were negative for E-cadherin whereas N-cadherin was upregulated (**Fig. S12B),** suggesting that collective migration of *oncostreams* proceeds in a manner akin to the collective migration of mesenchymal cells of the neural crest (*19*). BrdU staining showed no differences between *oncostreams* and *non-oncostream* regions, though the mitotic plane was always perpendicular to the main axis **(Fig. S12 C and D).**

As *oncostreams* are heterogeneous we tested their potential role in the dispersal of cells throughout the tumor. We designed co-implantation experiments using human glioma stem cells (MSP-12), and highly aggressive and *oncostream* forming glioma cells (GL26) co-implanted into immunosuppressed mice. Implantation of MSP12 cells alone generates slow-growing tumors (6-8 months to death). At 21 post-implantation MSP-12 cells remain restricted to the site of injection with an average distance of 28.9±7.73 µm from the actual injection site. Surprisingly, when MSP12 cells are co-implanted with GL26-citrine cells MSP-12 cells spread throughout the tumor moving along oncostreams to much longer distances (83.7±23.74 µm) from the injection site (**Figure 5D and 5E**). Cell processes from MSP12 cells implanted alone displayed a random distribution pattern. However, in co-implanted tumors, processes from MSP12 cells are completely aligned with glioma GL26 cells within *oncostreams* **(Fig. 5F and 5G)**. These results strongly suggest that *oncostreams* function as highways stimulating the rapid distribution of slow-moving glioma cells and/or non-tumor cells throughout the tumor mass. These findings help explain the mixing of different clonal populations seen in previous studies (*1, 20*) supporting a potential role of self-organizing *oncostreams* in determining spatial heterogeneity.

Interactions at the border: oncostreams foster glioma aggressiveness through collective invasion of the normal brain parenchyma

Finally, we asked whether *oncostreams* have promote glioma invasion. We found multicellular fascicles of elongated, aligned cells invading from the tumor border into the normal brain parenchyma; single cell invasion was also observed. (**Fig. 6A and Fig. S12C**).

We implanted glioma NPA GFP+ cells into mT/mG mice in which tdTomato (mT) red fluorescence expression is widespread in all cells/tissues to delineate tumor borders. We used our glioma organotypic model to analyze the invasion dynamics by time-lapse confocal imaging at the tumor border (**Fig. 6B**). We observed that glioma cells that extend from the tumor border to the normal brain parenchyma use different dynamic patterns, moving as isolated random cells and/or directional collective migratory structures resembling *oncostreams* structures similar to those in the tumor core (**Fig. 6, C to F and Fig. S13 to S16**).

To objectively distinguish between different dynamic patterns, we determined the angle velocity distribution, and the likelihood that either distribution corresponds to either a *stream*, a *flock*, or a *swarm*. We found *streams* following the perivascular niche, or invading brain parenchyma without following any pre-existing brain structures, as well as invading *flocks*, and *swarms* (**Fig. 6 C, E and F, and Fig. S14 to S16 A, C and D**). Glioma cells moving along blood vessels is consistent with previous studies (*21-23*). Relative position analysis (Fig. S13B) showed a high density of nearby neighbors within a distance lower than 40µm. Moreover, cell velocities were positively correlated (Fig. S13C) within this region.

Our data indicate the overall self-organization of collective motion at the glioma tumor border. We thus demonstrate the existence of an overall framework of self-organized collective motion at the glioma border, compared to previous descriptions (*23, 24*). Though the patterns observed at the tumor border are similar to those of the tumor core, cell speed differed between both areas. Cells in the tumor core display significantly lower average speeds (*stream*: 4.26; *flock*: 5.95, *swarm*: 6.27 µm/h) than cells at the tumor border or invading the normal parenchyma (*stream*: 7.95; *flock*: 7.55, *swarm*: 8.01µm/h) (**Fig. S17**). We conclude that oncostreams (*streams* and *flocks*) are self-organizing collective migratory structures that participate in the dynamic organization of the tumor microenvironment and promote invasion into the normal brain. Thus, *oncostreams* help determine glioma malignant behavior, and contribute to worsen clinical outcomes (**Figure 6G**).

DISCUSSION

Spatial tumor heterogeneity is an essential characteristic of tumor structure, that determines, in part, tumor malignant behavior (*25, 26*). How spatial heterogeneity is generated, however, remains poorly understood. Herein we demonstrated that tumor dynamics play a prominent role in the organization of spatial tumor heterogeneity.

We discovered the existence of a complex self-organizing network of collectively moving glioma cells, which we have termed *oncostreams*. These structures, fascicles of aligned, elongated cells, are present within the tumor core, and the tumor border and play a central role in the setting up of the typical spatial organization of tumor heterogeneity in gliomas, and thus, in the determination of overall glioma malignant behavior. The presence of self-organizing patterns of collective motion within gliomas define a novel dynamical aspect which we propose is central to the establishment of tumor heterogeneity.

In summary, our data demonstrate that glioma cells move throughout the tumor mass utilizing *streams* and *flocks*, as self-organizing patterns of collective motion. These collective dynamic patterns organize the complex glioma heterogeneity landscape and contribute to tumor development and invasion. Our findings open new paths to understanding dynamic glioma tumor cell migration and self-organization, and thus, novel approaches to understanding the malignant behavior of gliomas. We propose the targeting of *oncostreams* and glioma self-organization as a new approach to developing novel therapeutics for gliomas.

References and Notes

1. A. P. Patel *et al.*, Single-cell RNA-seq highlights intratumoral heterogeneity in primary glioblastoma. *Science (New York, N.Y.)* **344**, 1396-1401 (2014).
2. C. W. Brennan *et al.*, The somatic genomic landscape of glioblastoma. *Cell* **155**, 462-477 (2013).
3. R. B. Puchalski *et al.*, An anatomic transcriptional atlas of human glioblastoma. *Science (New York, N.Y.)* **360**, 660-663 (2018).
4. M. Ceccarelli *et al.*, Molecular Profiling Reveals Biologically Discrete Subsets and Pathways of Progression in Diffuse Glioma. *Cell* **164**, 550-563 (2016).
5. S. Jamous, A. Comba, P. R. Lowenstein, S. Motsch, Self-organization in brain tumors: How cell morphology and cell density influence glioma pattern formation. *PLoS computational biology* **16**, e1007611 (2020).
6. P. Friedl, D. Gilmour, Collective cell migration in morphogenesis, regeneration and cancer. *Nat Rev Mol Cell Biol* **10**, 445-457 (2009).
7. P. Rørth, Fellow travellers: emergent properties of collective cell migration. *EMBO Rep* **13**, 984-991 (2012).

8. E. Scarpa, R. Mayor, Collective cell migration in development. *J Cell Biol* **212**, 143-155 (2016).
9. T. S. Deisboeck *et al.*, Pattern of self-organization in tumour systems: complex growth dynamics in a novel brain tumour spheroid model. *Cell Prolif* **34**, 115-134 (2001).
10. Y. Jiao, H. Berman, T. R. Kiehl, S. Torquato, Spatial organization and correlations of cell nuclei in brain tumors. *PLoS One* **6**, e27323 (2011).
11. T. S. Deisboeck, I. D. Couzin, Collective behavior in cancer cell populations. *Bioessays* **31**, 190-197 (2009).
12. W. Bialek *et al.*, Statistical mechanics for natural flocks of birds. *Proceedings of the National Academy of Sciences of the United States of America* **109**, 4786-4791 (2012).
13. R. Staneva *et al.*, Cancer cells in the tumor core exhibit spatially coordinated migration patterns. *Journal of cell science* **132**, (2019).
14. A. Comba *et al.*, Fyn tyrosine kinase, a downstream target of receptor tyrosine kinases, modulates antiglioma immune responses. *Neuro-oncology* **22**, 806-818 (2020).
15. F. J. Núñez *et al.*, IDH1-R132H acts as a tumor suppressor in glioma via epigenetic up-regulation of the DNA damage response. **11**, eaaq1427 (2019).
16. D. J. Brat *et al.*, Comprehensive, Integrative Genomic Analysis of Diffuse Lower-Grade Gliomas. *N Engl J Med* **372**, 2481-2498 (2015).
17. D. W. Parsons *et al.*, An integrated genomic analysis of human glioblastoma multiforme. *Science (New York, N.Y.)* **321**, 1807-1812 (2008).
18. C. Koschmann *et al.*, ATRX loss promotes tumor growth and impairs nonhomologous end joining DNA repair in glioma. *Sci Transl Med* **8**, 328ra328 (2016).
19. E. Theveneau, R. Mayor, Neural crest delamination and migration: from epithelium-to-mesenchyme transition to collective cell migration. *Dev Biol* **366**, 34-54 (2012).
20. N. Bergmann *et al.*, The Intratumoral Heterogeneity Reflects the Intertumoral Subtypes of Glioblastoma Multiforme: A Regional Immunohistochemistry Analysis. *Front Oncol* **10**, 494 (2020).
21. D. Kedrin *et al.*, Intravital imaging of metastatic behavior through a mammary imaging window. *Nat Methods* **5**, 1019-1021 (2008).
22. G. J. Baker *et al.*, Mechanisms of glioma formation: iterative perivascular glioma growth and invasion leads to tumor progression, VEGF-independent vascularization, and resistance to antiangiogenic therapy. *Neoplasia* **16**, 543-561 (2014).
23. M. Alieva *et al.*, Intravital imaging of glioma border morphology reveals distinctive cellular dynamics and contribution to tumor cell invasion. *Scientific reports* **9**, 2054 (2019).
24. P. G. Gritsenko *et al.*, p120-catenin-dependent collective brain infiltration by glioma cell networks. *Nat Cell Biol* **22**, 97-107 (2020).
25. R. G. Verhaak *et al.*, Integrated genomic analysis identifies clinically relevant subtypes of glioblastoma characterized by abnormalities in PDGFRA, IDH1, EGFR, and NF1. *Cancer Cell* **17**, 98-110 (2010).
26. D. N. Louis *et al.*, The 2016 World Health Organization Classification of Tumors of the Central Nervous System: a summary. *Acta Neuropathol* **131**, 803-820 (2016).
27. T. J. Wilson, D. B. Zamler, R. Doherty, M. G. Castro, P. R. Lowenstein, Reversibility of glioma stem cells' phenotypes explains their complex in vitro and in vivo behavior: Discovery of a novel neurosphere-specific enzyme, cGMP-dependent protein kinase 1, using the genomic landscape of human glioma stem cells as a discovery tool. *Oncotarget* **7**, 63020-63041 (2016).
28. A. A. Calinescu *et al.*, Transposon mediated integration of plasmid DNA into the subventricular zone of neonatal mice to generate novel models of glioblastoma. *Journal of visualized experiments : JoVE*, (2015).

29. V. N. Yadav *et al.*, Molecular ablation of tumor blood vessels inhibits therapeutic effects of radiation and bevacizumab. *Neuro-oncology* **20**, 1356-1367 (2018).
30. E. Shelhamer, J. Long, T. Darrell, Fully Convolutional Networks for Semantic Segmentation. *IEEE Trans Pattern Anal Mach Intell* **39**, 640-651 (2017).
31. O. Ronneberger, P. Fischer, T. Brox. (2018).
32. M. Abadi *et al.*, in *12th {USENIX} symposium on operating systems design and implementation ({OSDI} 16)*. (2016), pp. 265-283.
33. M. Sharma, R. Pachori, U. R. Acharya, Adam: a method for stochastic optimization. *Pattern Recognit. Lett* **94**, 172-179 (2017).

Acknowledgments: We thanks all members of our laboratory for advice and comments on this work. **Funding:** This work was supported by National Institutes of Health, National Institute of Neurological Disorders and Stroke (NIH/NINDS) grants: R37-NS094804, R01-NS105556, R21-NS107894, R21-NS091555; R01-NS074387 to M.G.C.; National Institute of Neurological Disorders and Stroke (NIH/NINDS) grants: R01-NS076991, R01-NS096756, R01-NS082311 to P.R.L.; National Institute of Biomedical Imaging and Bioengineering (NIH/NIBI): R01-EB022563; National Cancer Institute (NIH/NCI) U01CA224160; Rogel Cancer Center at The University of Michigan G023089 to M.G.C. Ian's Friends Foundation grant G024230, Leah's Happy Hearts Foundation grant G013908, Pediatric Brain Tumor Foundation grant G023387 and ChadTough Foundation grant G023419 to P.R.L. RNA Biomedicine grant: F046166 to M.G.C. Health and Human Services, National Institutes of Health, UL1 TR002240 to Michigan Institute for Clinical and Health Research (MICHR), Postdoctoral Translational Scholars Program (PTSP), Project F049768 to A.C. **Author contributions:** Conception and design: A. Comba and P. R. Lowenstein. Development of methodology: A. Comba, P. J. Dunn, A. E. Argento, Todd Hollon, D.B. Zamler, P. R. Lowenstein. Acquisition of data, analysis, and interpretation: A. Comba, P. J. Dunn, A. E. Argento, Todd Hollon, D.B. Zamler, M.G. Castro, P. R. Lowenstein. Human histopathology analysis and identification of oncostreams: A. Comba, C. Kleer, A. E. Argento, P. R Lowenstein. Manuscript writing: A. Comba, M. G. Castro, P. R. Lowenstein. Review and/or revision of the manuscript: A. Comba, P. J. Dunn, A. E. Argento, Todd Hollon, D. B. Zamler, C. Kleer, M. G. Castro, P. R. Lowenstein. Administrative, technical, or material support (ie, reporting or organizing data, constructing databases): A. Comba, P. R. Lowenstein. Study supervision: M. G. Castro and P. R. Lowenstein. **Competing interests:** All authors of this paper declare no potential conflicts of interest. **Data and materials availability:** All data is available in the main text or the supplementary materials.

List of Supplementary Materials:

Materials and Methods

Figures S1-S17

Tables S1-S4

Movies S1-S8

References (*27-33*)

Fig. 1

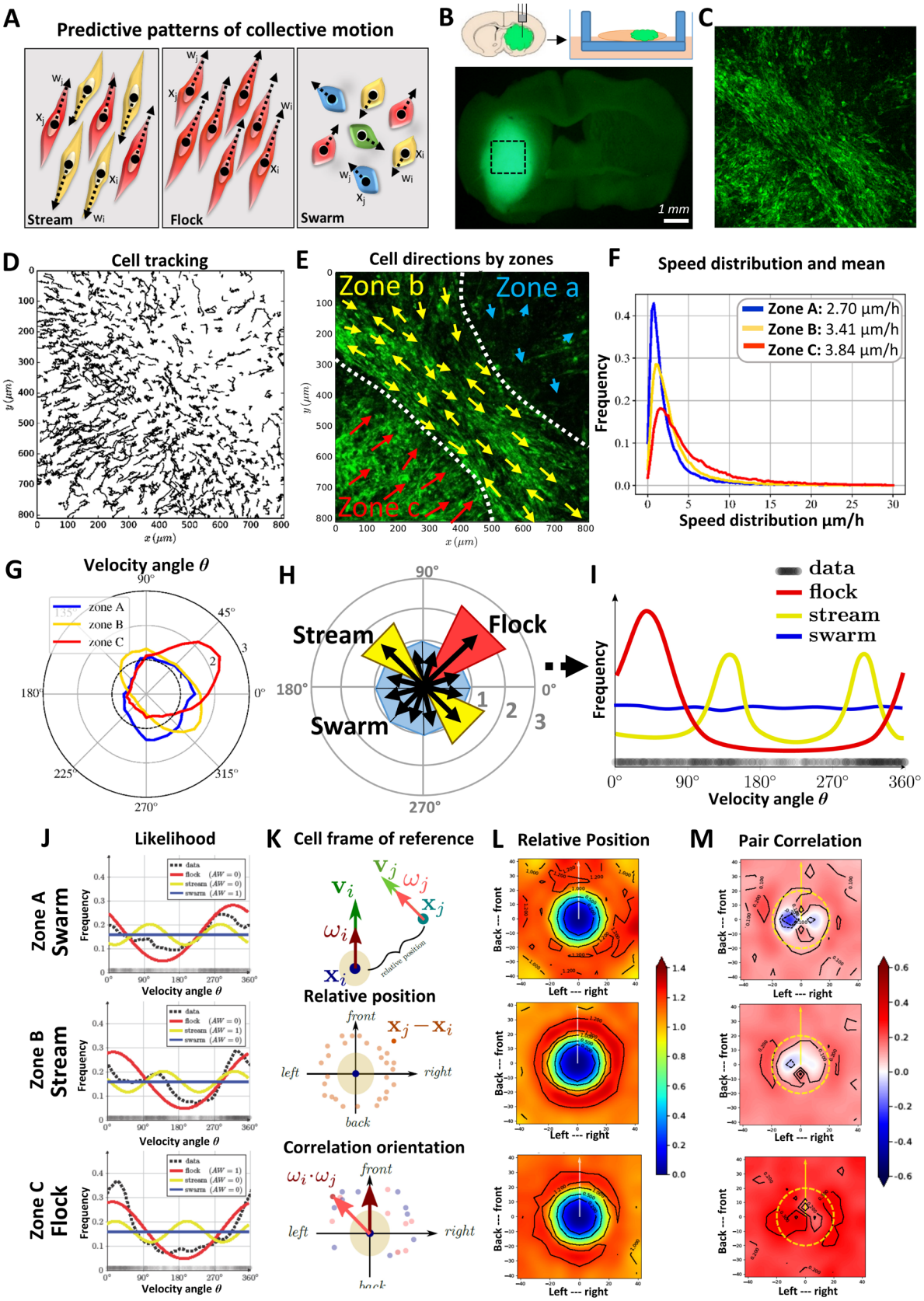

Fig. 1. Gliomas exhibit complex self-organized dynamic patterns within the tumor core. A) Dynamic self-organizing collective motion patterns predicted by our *in silico* agent-based modeling (*5*), in which cell eccentricity and density determine pattern formation: 1. *stream* (↑↓), 2. Flock (↑↑), 3. Swarm (↕↔). **B)** Experimental setup: NPA-GFP glioma cells were intracranially implanted in C57BL6 mice. Organotypic slice cultures were used for confocal time-lapse imaging of the tumor core. **C)** Single representative time-lapse confocal image of glioma cells within the tumor core. **D)** Tracking analysis of individual cell paths performed using the Track-Mate plugin from Image-J. **E)** Preferred direction of cells within three zones superimposed onto a representative time lapse-image. **F)** Speed distribution and mean speed ($\mu m/h$) in Zones A, B and C. **G)** Distribution of angle velocity for each zone. The angle velocity of each cell is described by a unique angle denoted θ. Plot shows proportion of cells moving in every direction for each zone. **H-I)** Classification of collective motion patterns: *stream*, *flock* or *swarm*. The distribution is *uni-modal* for a flock (only one peak) whereas it is *bi-model* for a stream (two peaks). For a *swarm*, the distribution is *flat* (no preferred angle velocity). In **(I)** angle velocity was transformed to a histogram; these data were then used to calculate the likelihood that a particular distribution of angle velocities corresponds to either a *stream*, a *flock*, or a *swarm*. The results are given in **(J)** for each zone. The frequency distribution of the data (shown in black lines) uses a *non-parametric* estimation (kernel density estimator). We tested three types of distributions ρ to describe the data-sets and give a *likelihood* in each case. The best fit was then determined by the Akaike Weight (AW). **K)** Illustration of the method used to determine relative position and pairwise correlation of orientation. **L)** Frequency for each zone of the relative position between two cells. In the frame of a reference of one cell, we estimate the probability to have another cell x_j nearby. **M)** Pair-wise correlation with nearby neighbors. Depending on the relative position $\mathbf{x}_j$-$\boldsymbol{x}_j$, we estimate the correlation between the velocity directions $\boldsymbol{\omega}_i$ and $\boldsymbol{\omega}_j$. Axes indicate cell position and distance in μm of the neighboring cells. Dotted yellow line show the average size of the centered cell.

Fig. 2

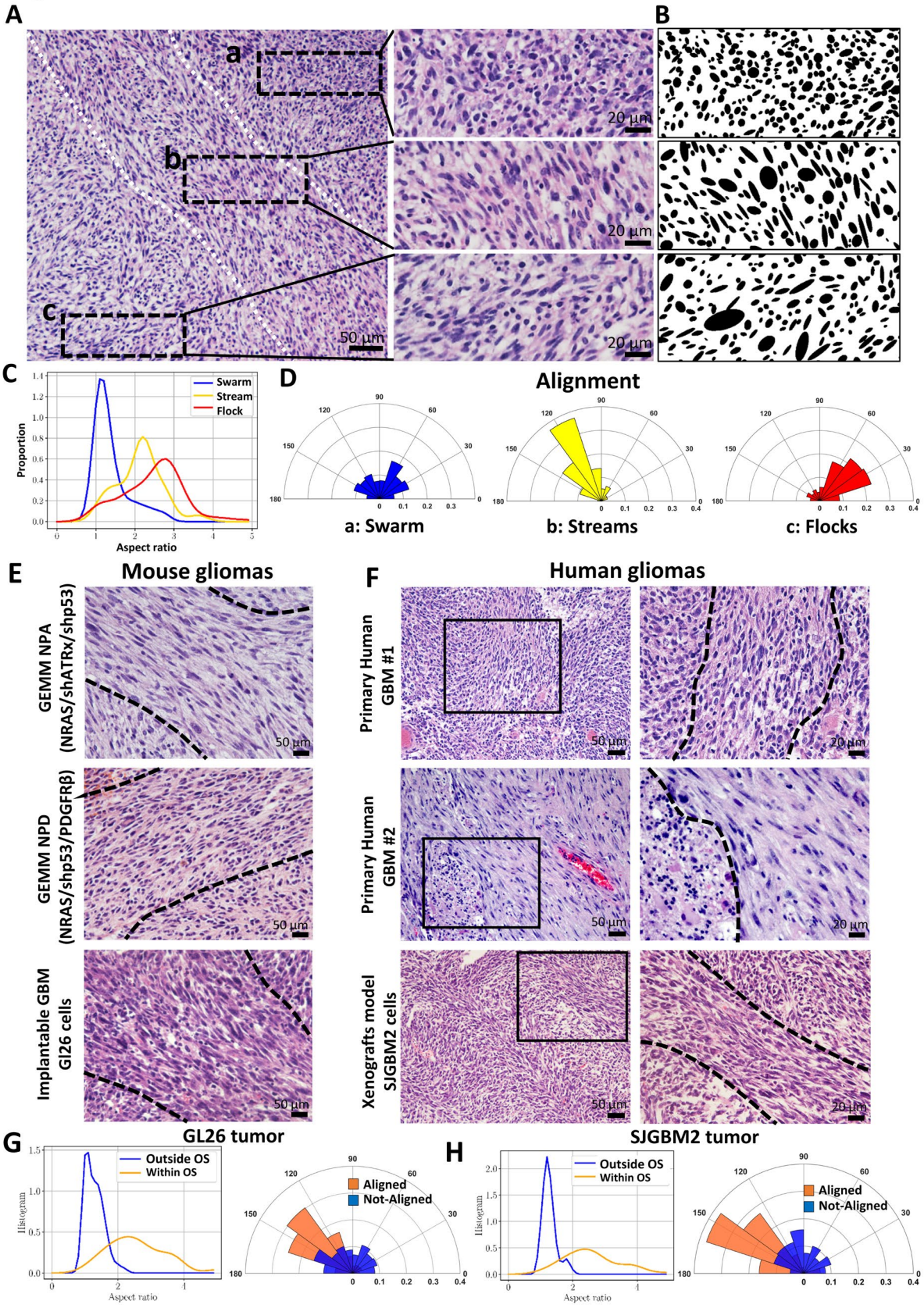

Fig. 2. Collective migratory multicellular structures, oncostreams, are present in mouse and human gliomas. A) H&E staining of a 5µm microtome section taken from an organotypic slice culture glioma model used for confocal imaging, and shown in **Fig. 1C, E**. Dotted white lines define different zone which display different dynamic patterns in **Fig. 1E**, i.e., a=*swarm*, b=stream and c=flock, and boxes are shown at higher power to the right. **B)** Masks generated by particle analysis in Image J were used to calculate the alignments shown in Fig. 2D. **C)** Histogram of cell eccentricity analysis of organotypic H&E stained glioma sections. Aspect ratio of cells are shown for a swarm (blue; ~1), a stream (yellow; >2) and a flock (red; >2). **D)** Alignment analysis of cells: Angle histogram plots show areas of high proportion of aligned cells (stream and flock) (narrow range of angle orientation), and areas of no preferred orientation (swarm).**E)** Representative 5µm H&E microtome sections from gliomas showing that elongated glioma cells forming oncostreams (dotted line) are present in several genetically engineered mouse glioma models (GEMM) such as NPA (NRAS/shATRx/shp53) and NPD (NRAS/shp53/PDGFβ), and the GL26 intracranial implantable model of glioma. Scale bars: 20 µm. **F)** Representative 5µm H&E microtome sections of human glioma (top, middle), and human xenografts (bottom) showing the presence of oncostreams. Scale bar: left 50 µm and right 20 µm. **G-H)** Histograms of cellular shape analysis (aspect ratio) and angle orientation (alignment) shows areas of oncostreams (OS) formed by elongated and aligned cells and areas with no oncostreams (No-OS) rounded and not-aligned cells.

Fig. 3

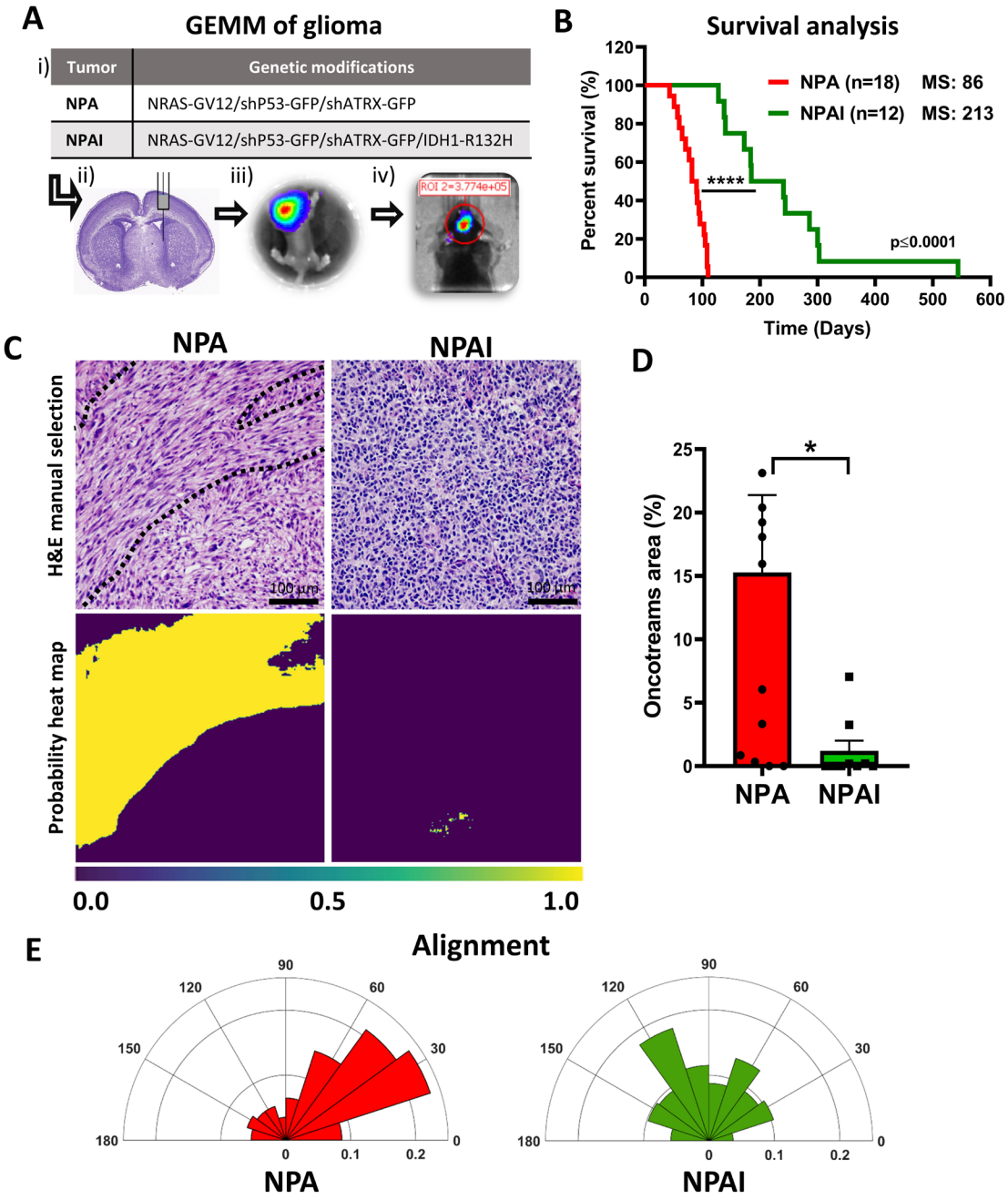

Fig. 3. The density of oncostreams correlates positively with tumor malignancy in mouse genetic engineered glioma models. A) Schematic representation of the GEMM of glioma generated using the Sleeping beauty transposase system; i) genetic makeup of NPA and NPAI gliomas, ii) plasmid injection into the lateral ventricle of neonatal mice; iii) bioluminescence imaging of a neonatal mouse 1-day post injection, iv) bioluminescence detection at 70 days post-injection. **B)** Kaplan–Meier survival plots of NPA and NPAI mouse gliomas shows that animals bearing IDH1-R132H mutant tumors have prolonged median survival (MS): **NPA** (MS: 86 days; n: 18) versus **NPAI** (MS: 213 days; n:12). Log-rank (Mantel-Cox) test; ****$p<0.0001$. **C-D)** Deep learning method for oncostream detection on H&E stained mouse glioma sections: **C)** Representative images of oncostreams manually segmented on H&E stained sections of NPA gliomas (first row). The output of our trained model for each image is shown below (probability heat maps). for tissue containing oncostreams (NPA), and not (NPAI), scale bar = 100 μm. **D)**. Fourteen random fields per tumor section per animal were imaged, n=9 and 12 per condition and analyzed by deep learning analysis. Error bars represent ± SEM; unpaired t-test analysis, *$p<0.05$. **E)** Angle histogram plots shows aligned cells in NPA tumors vs non-aligned cells in NPAI glioma sections.

Fig. 4

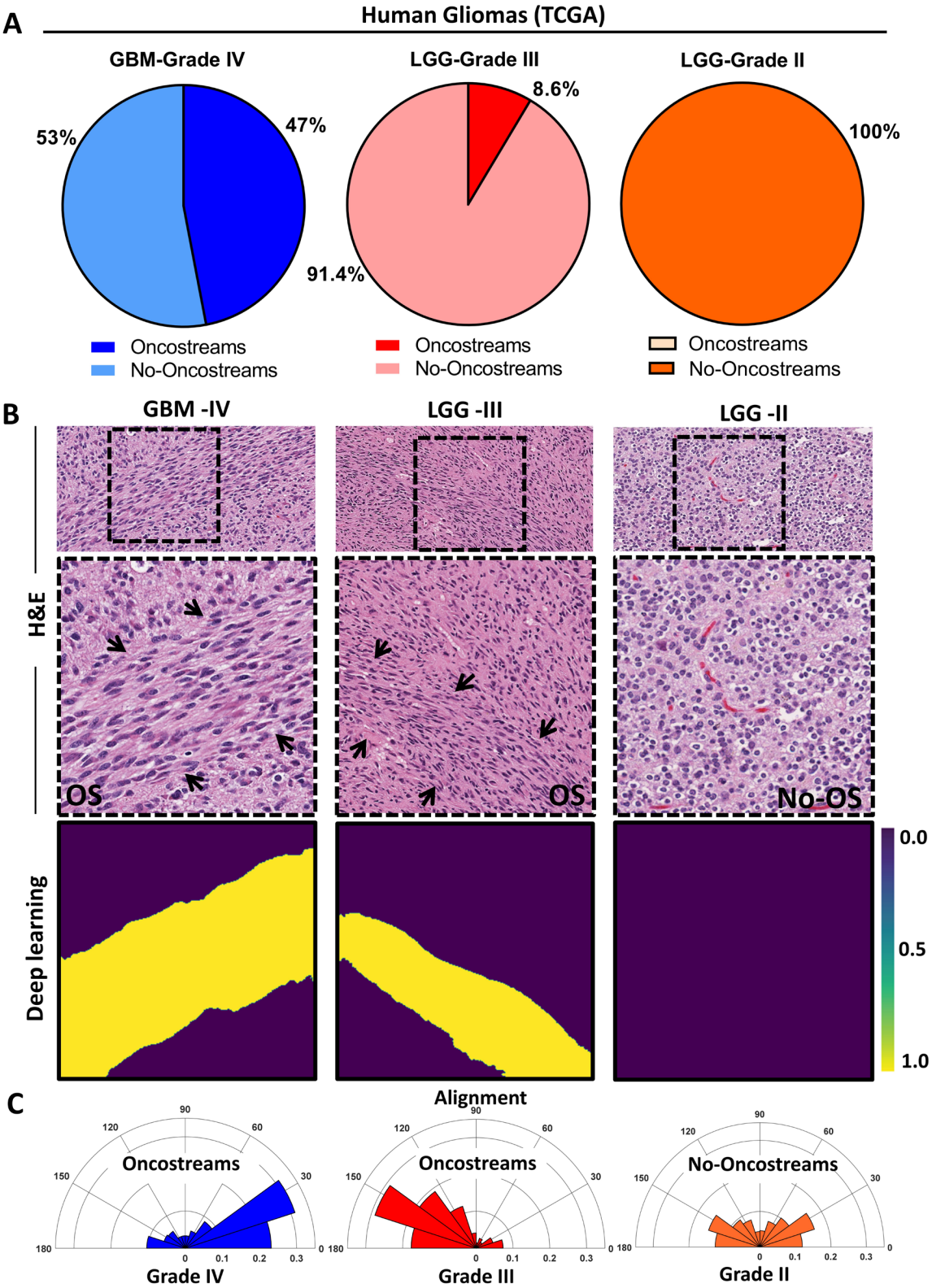

Fig. 4. The density of oncostreams correlates positively with tumor grade in human gliomas. **A)** Pie charts show percentage of tumors displaying oncostreams in relation to tumor grade. Oncostreams are present in 47% of GBM grade IV tumors, 8.6 % of LGG grade III, and are absent in LGG histology grade II. **B)** Low (first row) and high (second row) magnification of H&E images are shown for gliomas WHO grade IV, III, II from TCGA. Deep learning analysis for each of the high magnification images is shown in the third row. Our model was able to detect oncostreams in grade IV and III but not in grade II gliomas. **C)** Angle histogram plots show the alignment of cells on H&E histology sections of Grade IV and Grade III gliomas' oncostreams and random alignment in grade II glioma sections lacking oncostreams.

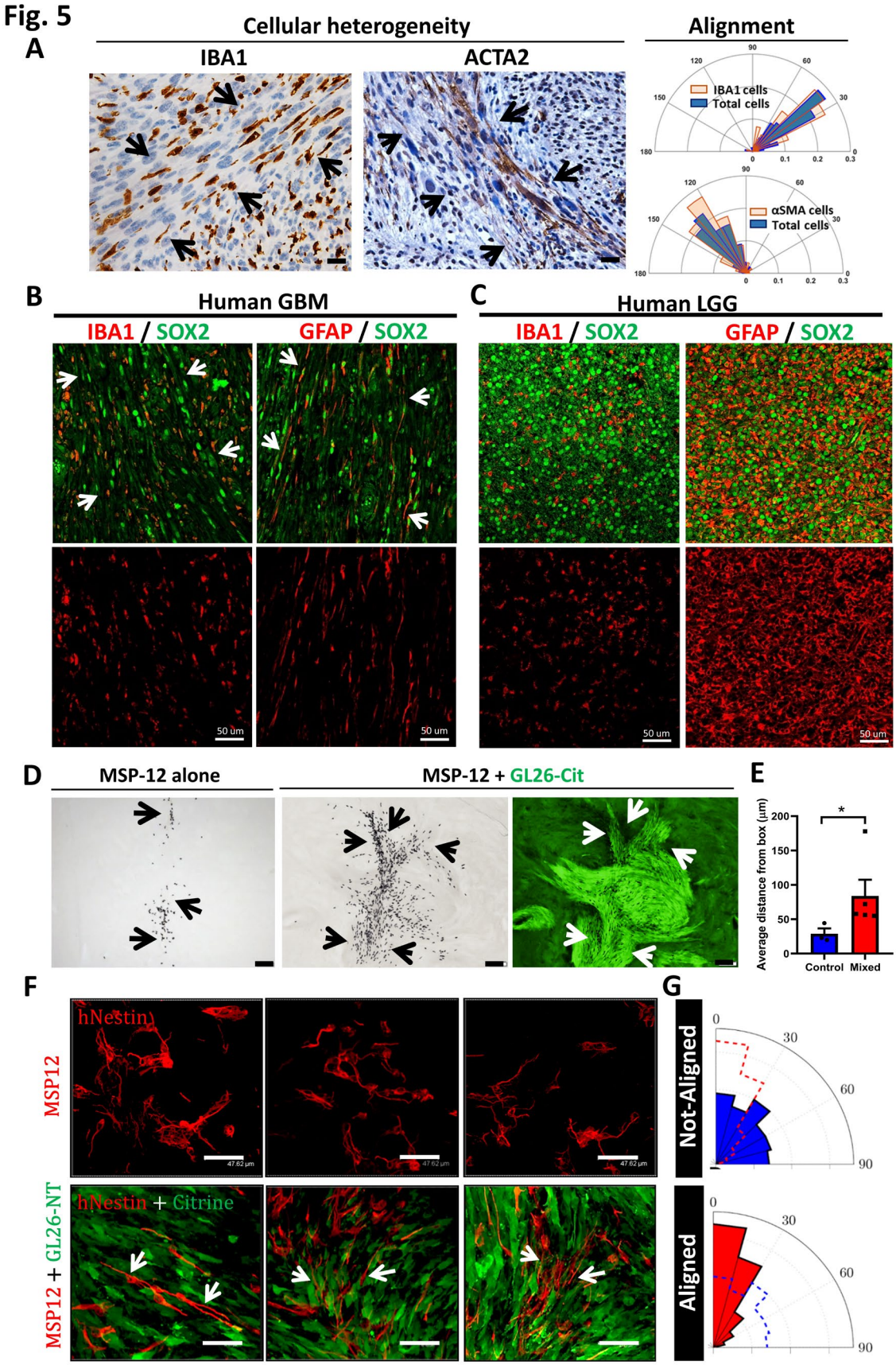

Fig. 5. Oncostreams are heterogeneous and assist intratumoral distribution of tumor and immune cells. A) Angle histogram plots show that tumor cells, microglia/macrophages (IBA1+), and mesenchymal cells (ACTA2+), are all within, and aligned with, the main orientation axis of oncostreams. Scale bar: 20 µm. **B-C)** Immuno-fluorescence staining of SOX2+ tumor cells (green), glial fibrillary acidic protein (GFAP+) cells (red), and microglia/macrophages (IBA1+) cells (red) in human glioblastoma GBM WHO Grade IV, IDH-WT **(B)** and in low grade glioma (LGG) IDH-mutant **(C)**. Scale bars: 50 µm. **D)** Co-implantation of high malignant GL26-citrine cells (green) and human MSP12 glioma stem cells (ratio 1:30), and MSP12 cells alone (control). Immuno-histochemistry of human nuclei (black) denote MSP12 cells. Arrows show MSP12 distribution within the brain or the tumor. Scale bar: 100 µm. **E)** Quantification of MSP12 distance from the site of implantation. n=3 for control and n=5 for co-implantation (MSP12+GL26). Error bars ± SEM; t-test analysis, *$p<0.05$. **F)** Immuno-fluorescence images of human-Nestin (red) indicating MSP12 cells, and GL26-citrine cells. Note that MSP12 cells have a multipolar structure when alone, but a mainly bipolar structure when aligned to GL26-citrine cells. Scale bar: 47.62 µm. **G)** Angle histogram plots show the quantified alignment of MSP12 with GL26 cells within oncostreams and no alignment of MSP12 cells implanted alone.

Fig. 6

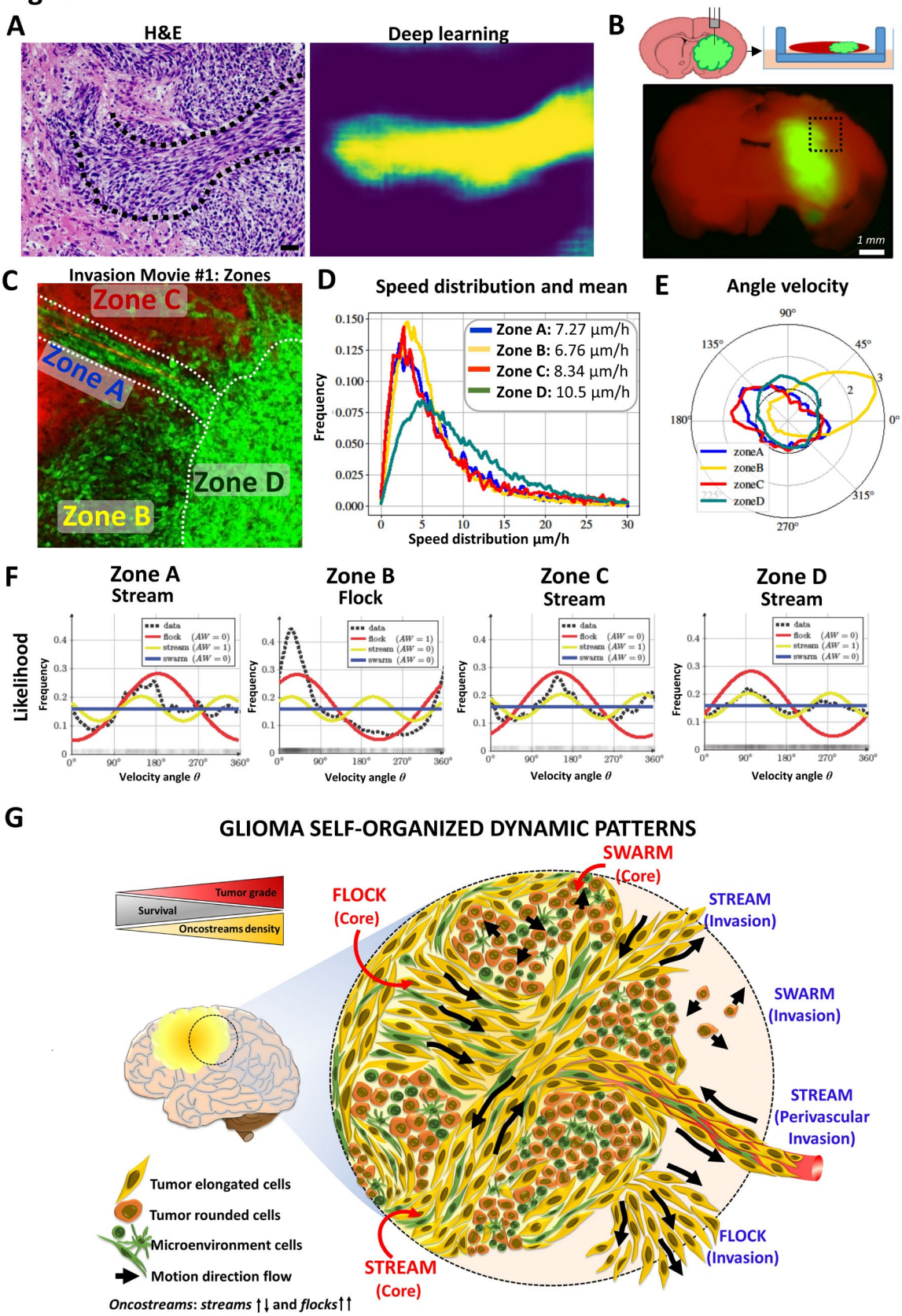

Fig. 6: Oncostreams contribute to glioma malignant behavior at the tumor invasive borders. **A)** Representative images of *oncostream* invasion (dotted line indicating an oncostreams at the tumor border) on H&E stained sections of NPA gliomas (left), and its detection by deep learning analysis. Scale bar=20 μm. **B)** Schematic representation of location of imaging of tumor borders. **C)** Representative time-lapse scan confocal image of glioma cells at the tumor border, taken from border movie #1. **D)** Histogram of speed distribution and mean speed ($\mu m/h$) of Zone A, B, C and D. **E)** Angle Velocity distribution analysis (θ) performed by zones. Plot shows overall direction and magnitude of cells' movement. **F)** Likelihood analysis of the dynamic patterns at the tumor border. Graph of density estimation ρ *flock* (red), ρ *stream* (yellow) and ρ *swarm* (blue). The estimation in black line uses a *non-parametric* estimation. AW: 0 or AW:1. **G)** Schematic representation of self-organized patterns of collective migration in highly malignant gliomas. Our study defines the existence of three types of collective patterns at the tumor core (in red font), and at the tumor border (in blue font), i.e., streams, flocks, and swarms.